Magnetic Interactions in Spin Labeled Au Nanoparticles

V. Lloveras,[†,‡] *E. Badetti*,[†,‡] *V. Chechik*,*[¥] *J. Vidal-Gancedo**[†,‡]

[†]Institut de Ciència de Materials de Barcelona (ICMAB-CSIC), Esfera UAB; Campus UAB s/n; E-08193 Cerdanyola del Vallès, Spain

[‡]CIBER de Bioingeniería, Biomateriales y Nanomedicina (CIBER-BBN); Barcelona, Spain.

[¥] Department of Chemistry, University of York; YO10 5DD Heslington, York, UK

ABSTRACT

A series of gold nanoparticles functionalised with TEMPO-modified disulfide 2 have been prepared and studied by Electron Paramagnetic Resonance (EPR) spectroscopy, UV-Vis, TEM microscopy, Energy Dispersive X-ray analysis (EDX) and Thermogravimetric Analysis (TGA). In order to increase the packing of spin labels on the particle surface, heat-induced size evolution and ligand exchange reactions were used. The optimised synthesis included a one-pot reaction at room temperature that led to gold nanoparticles with a controlled large size (*ca.* 7 nm) and high

coverage of radicals. These nanoparticles showed a $|\Delta m_s| = 2$ transition at half-field which gives direct evidence of the presence of a high-spin state and permits an EPR study of the nature of the magnetic coupling between the spins. The results showed dominant antiferromagnetic interactions between radicals but at lower temperatures a ferromagnetic contribution was observed.

Keywords: Gold nanoparticles, organic radicals, high coverage, EPR, magnetic properties

INTRODUCTION

Suparmolecular magnetic assemblies can be built using a range of different materials as scaffolds: functionalised polymers,[1,2] dendrimers[3-5] or metallic nanoparticles. In this work, we used gold nanoparticles as supports for organic radicals to study magnetic interactions. There are only a few reports on spin-labeled gold nanoparticles[6-13] concerning the synthesis, mechanistic pathways, bioimaging and nanotherapeutic applications, catalysis etc. The dipole-dipole and exchange interactions between adjacent radicals adsorbed on the same nanoparticles have been explored.[7] However, a half-field transition signal has never been observed in the EPR spectra of these systems, and the study of magnetic interactions between radicals anchored onto a gold nanoparticle still remains a challenging goal.[13] To achieve this goal, it is necessary to obtain a high density of radicals on the nanoparticle surface. As the nanoparticle curvature decreases with increased particle size, larger particles are expected to show tighter packing of ligands. Therefore, the synthesis of large nanoparticles with high coverage of spin labels is required.

Gold nanoparticles (Au NPs) have high stability, they are relatively easy to prepare and functionalize[14] and hence are promising building blocks for designing new materials.[15] They have many potential applications in gold nanomedicine,[15,16] as biosensors,[16] in cancer therapy,[17-

[19] catalysis,[11,20] optoelectronics,[21] spintronics[22] etc. The most commonly used synthetic methods for the preparation of gold nanoparticles are based on the reduction of gold salts in organic solvents in the presence of surface stabilizing ligands, which prevent aggregation of the particles by electrostatic and/or steric repulsion.[15] The two-phase procedure, first published in 1994 by Brust and co-workers, allows a facile synthesis of stable thiol protected Au NPs with controlled size and dispersity.[23] Since then, this procedure has been applied as the starting point in many experiments. For example, alkanethiol-protected Au NPs were used in a number of ligand exchange reactions to synthesize nanoparticles with various functionalities.[24]

The spin-labeled gold nanoparticles prepared via the exchange reaction of ligands on the Au NPs surface such as alkyl thiolates or phosphines, with TEMPO-substituted disulfide was first reported in 2002.[25] By controlling the stoichiometry of the ligand-exchange reaction it was possible to modulate the Au nanoparticles coverage of nitroxides. However, since disulfide ligands show poor reactivity in exchange reactions with thiol-protected nanoparticles, only a small number of spin-labeled ligands (<10) can be adsorbed on a nanoparticle in this way, preventing high coverage.[26] Uniform coating shells can only be formed when a large excess of the incoming ligand is used in the exchange reaction,[27] otherwise, an incomplete ligand exchange takes place and, as a result, randomly organized monolayers are formed. Au nanoparticles protected by weaker bound ligands such as phosphines or amines are much more prone to exchange and can be used to prepare higher coverage spin labelled particles.[26,28]

Monolayer protected gold nanoparticles synthesis usually results in the formation of small particles, 1-3 nm in diameter. In order to reduce the nanoparticle curvature, their diameter should be increased. A number of methods have been developed to tune the particle dimensions.[29] The most commonly used procedures involve two-phase synthesis and subsequent digestive ripening,[30,31] a seeding growth strategy[32,33] or a combination of both approaches.[34,35]

Herein, we combine different methodologies and report three strategies for producing large nanoparticles, up to *ca.* 7 nm in diameter, with high coverage of a TEMPO-modified ligand. In these strategies, the exchange reaction is performed starting from thiol, phosphine and amine-protected Au nanoparticles and using disulfide-TEMPO modified ligand **2** as a spin-labeled ligand. The magnetic interactions between radicals anchored onto the surface of such nanoparticles have been explored by EPR.

MATERIALS AND MEASUREMENTS

Solvents and starting materials were purchased from Aldrich. The reactions and the column chromatography were monitored by TLC using aluminium plates covered with silica 60 F_{254} Merck. Silica column chromatography was carried out using silica gel 60 (35-70 mesh). Spin-labeled Au nanoparticles were purified by gel permeation chromatography using Bio-Beads SX-1 (Bio-Rad) gel and dichloromethane or toluene as eluent. IR spectra were recorded in the attenuated total reflectance mode (ATR) in a Perkin Elmer Spectrum One Fourier transform spectrometer. UV-Vis measurements were performed using a UV-Vis-NIR Varian Cary 5000 Espectrophotometer. EPR spectra were obtained with an X-Band Bruker ESP 300E spectrometer equipped with a TE102 microwave cavity, a Bruker variable temperature unit, a field frequency lock system Bruker ER 033 M; line positions were determined with an NMR Gaussmeter Bruker ER 035 M. The modulation amplitude was kept well below the line width, and the microwave power was well below saturation. HR-TEM analyses were performed in the "Servei de Microscòpia" of the Universitat Autònoma de Barcelona using a JEOL JEM-2010 model at 200 kV.

Details of the nanoparticle synthesis are available in the Supporting Information.

RESULTS AND DISCUSSION

Preparation of thiol- and phosphine-protected gold nanoparticles with high coverage of TEMPO-modified ligand by a three-step procedure. Preparation of high coverage Au NPs by direct reduction of $AuCl_4^-$ in the presence of the spin labeled disulfide 2 was not possible due to the degradation of the spin label under these conditions (Scheme S1 in the SI). Therefore, we decided to use ligand exchange reaction. In this case, the synthesis of thiol- and phosphine-protected spin-labeled gold nanoparticles produced small NPs with low and intermediate coverage of spin-labels, respectively. A heat treatment in the presence of excess of spin labeled ligand 2 was performed in order to increase both the size of these nanoparticles and spin label coverage.

n-Buthanethiol protected Au nanoparticles 1 were synthesized using Brust's method[23] with 1:1 thiol:Au ratio (reaction 1.1 of Scheme 1). Disulfide TEMPO-modified spin label 2 was synthesized following a procedure described previously.[26] The ligand exchange reaction between disulfide 2 and particles 1 was carried out overnight at 32 ºC, with 100:1 bis-nitroxide disulfide/Au ratio (reaction 1.2 of Scheme 1). The concentration of nanoparticles was calculated assuming a molecular formula $Au_{300}R_{100}$, where R is the alkanethiol ligand.[26] The obtained nanoparticles 3 were purified by gel permeation chromatography.

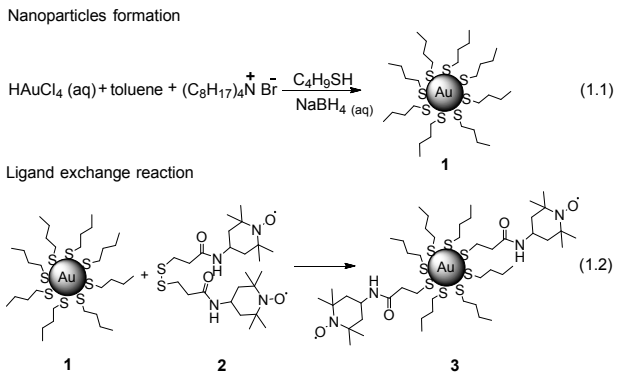

Scheme 1. Synthesis of spin-labeled gold nanoparticles 3.

The solution EPR spectrum of nanoparticles 3 (Figure 1a) showed a three-line pattern with selective broadening of the high-field line. The free radical signal is split into a triplet due to the interaction with the ^{14}N nuclei (I_n = 1), with a hyperfine constant of 15.5 G, typical of TEMPO derivatives. The lower height of the high field line in the spectrum is due to the hindered motion of a nanoparticle-attached spin label, resulting in incomplete averaging of anisotropic components of the *A* and *g* tensors. No apparent contribution of any broad EPR line was observed, attributed to nearly uniform low coverage of isolated spin labels with no appreciable interactions between the radicals adsorbed on the same particle. The UV-Vis spectrum (Figure 1b) showed a very weak plasmon peak (shoulder at around 520 nm) indicating the formation of quite small nanoparticles.[36,37] The shape and position of this band was in agreement with previously reported particles of *ca.* 2-nm diameter synthesized by the two-phase method.[23,38] In fact, as determined by TEM microscopy, these gold nanoparticles had a diameter of 2.4 ± 0.6 nm (see the Supporting Information).

In order to increase the size and spin label coverage of the obtained nanoparticles, they were subjected to heat treatment in the solid state.[39] The optimal conditions found were the addition of tetraoctylammonium bromide and ligand 2 to the small thiol-protected spin-labelled Au nanoparticles 3 followed by heat treatment in the solid state at 130 ºC for 1 h under nitrogen atmosphere (see reaction 1.3). Previously, the stability of the starting material (nanoparticles 3) was tested by heating a small amount to 130 ºC for 50 min under inert atmosphere. The EPR spectrum confirmed its stability showing the same spectrum shape and intensity before and after the heat treatment. The heat-treated nanoparticles 3T were washed with methanol and purified by gel permeation chromatography.

Heat treatment in the solid state

$$\underset{\text{(low coverage)}}{\text{Au NP (3) + TOABr + ligand 2}} \xrightarrow[N_{2(g)}]{\text{1h, 130°C}} \underset{\text{(high coverage)}}{\text{Au NP (3T)}} \qquad (1.3)$$

Interestingly, the solution EPR spectrum of gold NP 3T at room temperature showed a spectral pattern dominated by a single, intense broad line with peak-to-peak linewidth *ca.* 16.5 G (Figure 1c). This change in the shape of the spectra is due to dipole-dipole and exchange interactions between adjacent radicals adsorbed on the same nanoparticle and the decrease in the corresponding radius of curvature; this implies that the spin label coverage of the nanoparticles has dramatically increased.

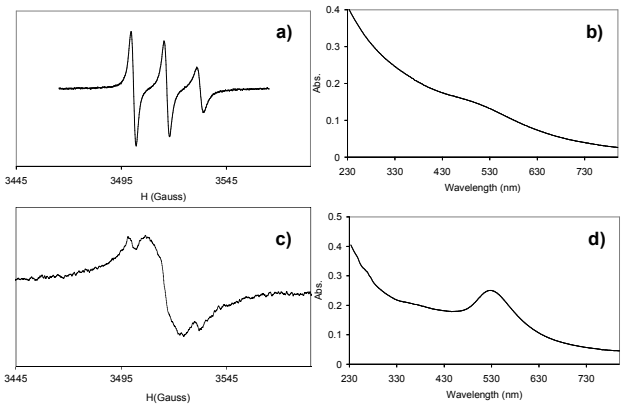

Figure 1. EPR (a, c) and UV-Vis spectra (b, d) of Au NPs 3 before the heat treatment (a, b) and nanoparticles 3T after heat treatment (c, d), in CH_2Cl_2 at room temperature. We have changed Figure 1c with the correct magnetic field scale.

The UV-Vis spectrum of nanoparticles 3T (Figure 1d) showed a surface plasmon (SP) peak at *ca.* 525 nm, much more pronounced than in nanoparticles 3 before the heat treatment (Figure 1b). The increased intensity of the SP band, without an apparent shift in energy, is indicative of an increase in core size.[23,40] In fact, as determined by TEM microscopy, these gold nanoparticles

had a diameter of 5.6 ± 0.9 nm (Figure 2). Thus, the heat treatment resulted in the nanoparticles size increase by a factor of 2.8 (from ~ 2 to 5.6 nm), as well as spin label coverage. The electron diffraction of this sample (Figure 2d) showed the characteristic pattern of face-centred cubic (fcc) gold(0) (see the SI). EDX spectrum confirmed the presence of S-ligands in the NPs (see the Supporting Information).

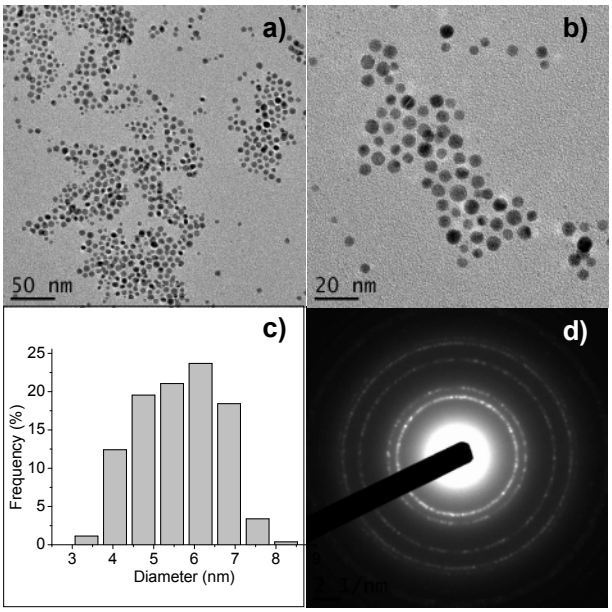

Figure 2. a) and b) TEM pictures of nanoparticles 3T obtained after the heat treatment. c) Core size distribution histograms of the nanoparticles. d) Electron diffraction patterns corresponding to Au(0) fcc of the nanoparticles.

Au nanoparticles protected by triphenylphosphine 4 were synthesized using published procedures (reaction 1.4 of Scheme 2).[41] Spin-labeled nanoparticles 5 were prepared by a ligand-exchange reaction between the triphenylphosphine-protected Au nanoparticles 4 and *ca.* 100 fold excess of bis-nitroxide 2 (reaction 1.5 of Scheme 2). The reaction was stirred overnight at room temperature and the nanoparticles were purified by gel permeation chromatography.

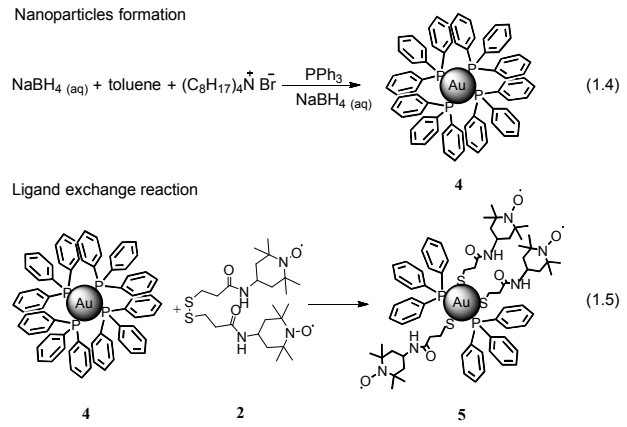

Scheme 2. Synthesis of spin-labeled gold nanoparticles 5.

In this case, due to the high lability of the phosphine ligands as compared to thiols,[26,28] it was expected that more triphenylphoshine ligands would be replaced by the disulfide ligand. In fact, the solution EPR spectrum of nanoparticles 5 (Figure 3a) showed a broad line overlapping three narrower lines, indicating that spin-labeled nanoparticles with intermediate-high coverage were formed. The UV-Vis spectrum (Figure 3b) showed no visible plasmon resonance peak, indicative of gold nanoparticles with < 2 nm in diameter.[42] In fact, as determined by TEM microscopy, these gold nanoparticles had a diameter of 1.4 ± 0.3 nm (see the Supporting Information).

In order to increase the size and spin label coverage of nanoparticles 5, we followed the same strategy as before, e.g., heat treatment in the solid state (see reaction 1.6).

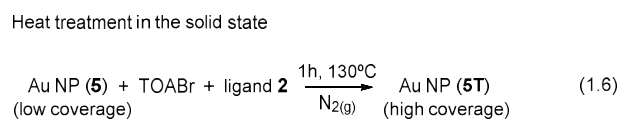

The solution EPR spectrum of the heat-treated nanoparticles 5T at room temperature showed a spectral pattern dominated by a single broad line with a line width of *ca.* 13.5 G (Figure 3c). This

change in the spectrum shape before and after the heat treatment (Figure 3a and 3c) indicates that the spin label coverage of the nanoparticles was substantially increased during the process.

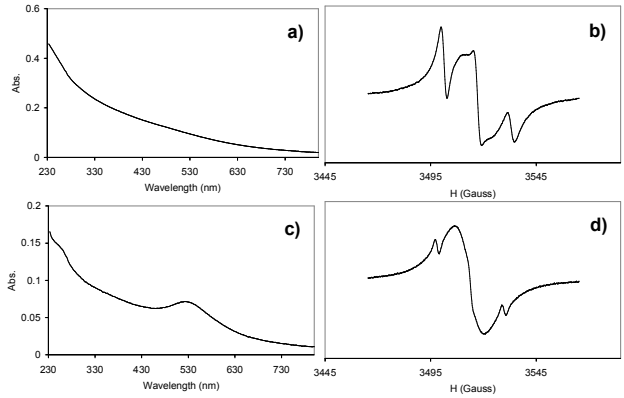

Figure 3. UV-Vis-(a, c) and EPR (b, d) spectra of gold nanoparticles 5 before the heat treatment (a, b), and nanoparticles 5T after heat treatment (c, d) in CH_2Cl_2 at room temperature.

The UV-Vis spectrum of nanoparticles 5T showed a large surface plasmon peak at *ca.* 525 nm (Figure 3d). This suggests that in this case, the heat treatment also produced larger nanoparticles. However, the SP peak was less pronounced than in the heat-treated nanoparticles 3T (Figure 1d). A representative TEM (Figure 4) showed homogeneous and well dispersed gold nanoparticles with a diameter of 3.2 ± 0.7 nm. EDX spectrum confirmed the presence of the two types of ligands in the NPs: thiol- TEMPO derivative and phosphine- (see the Supporting Information).

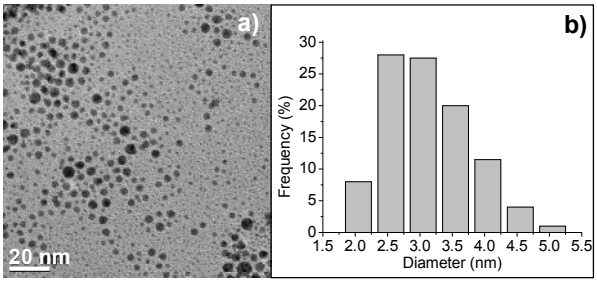

Figure 4. a) TEM pictures of Au nanoparticles 5T obtained after the heat treatment process and b) core size distribution histograms of these nanoparticles.

Preparation of tri-*n*-octylamine-protected gold nanoparticles with high coverage of TEMPO-modified ligand by a single-step procedure. Apart from using thiols and phosphines, we tried amines as sacrificial stabilizing ligands for Au nanoparticles, as they are weakly bound and prone to exchange. We also aimed to develop a shorter method than the three-step procedure described above (e.g., generation of thiol- or phosphine-protected Au NPs, ligand exchange reaction and heat treatment). With these considerations in mind, the best sacrificial amine for our purpose was tri-*n*-octylamine and the optimised protocol was as follows: the tri-*n*-octylamine stabilized gold nanoparticles were prepared following a one-phase procedure,[35] then, after a reduction with $NaBH_4$, spin label **2** was added to the same reaction flask (reaction 1.7). Finally, the reaction was let stirring at room temperature overnight and the nanoparticles were precipitated with methanol and purified by gel permeation chromatography.

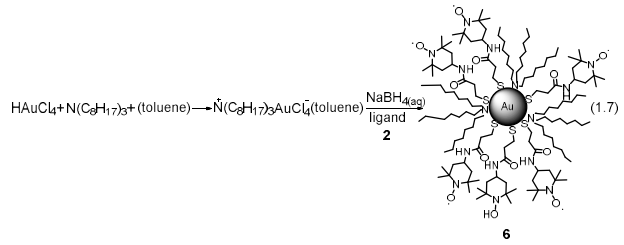

Interestingly, the solution EPR spectrum of the obtained nanoparticles 6 (Figure 5a) showed a single broad line, with a linewidth of *ca.* 11.5 G. This is the narrowest linewidth obtained in all our experiments (e.g., the linewidth of the broad line was 16.5 and 13.5 G for nanoparticles 3T and 5T, respectively, see Figure S1 in the SI). As the width of the broad line component in such spectra is sensitive to the density of the spin labels on the NP surface,[26] at high coverage of spin labels the broad line becomes narrower, which is similar to the exchange-narrowing effect observed in the EPR of solid samples.[43] The radical ensembles become larger, more compact and therefore more uniform. The one-pot procedure thus led to the nanoparticles 6 with the highest coverage of radicals as well as the tightest packing. Moreover, the very pronounced surface

plasmon band observed by UV-Vis spectroscopy at *ca.* 530 nm (Figure 5b) indicated that considerably larger nanoparticles were formed. In fact, TEM microscopy showed nanoparticles with a diameter of 6.7 ± 1.5 nm (Figures 5c-5e), which was larger than that obtained with the thiol- and phosphine-protected nanoparticles after the heat treatment (5.6 and 3.2 nm for nanoparticles 3T and 5T, respectively). EDX spectrum confirmed the presence of sulphur and nitrogen atoms (see the Supporting Information).

It is worth mentioning that this method leads to spin-labeled Au NPs in a one-pot reaction. Moreover, the obtained nanoparticles have both high coverage of spin labels and a relatively large size (with the corresponding decrease in the radius of curvature) [44] without the requirement for any further treatment. To the best of our knowledge, there is only one example of a one-pot synthesis of spin-labeled AuNPs in the literature.[10] However, in that case the nanoparticles were small (2 nm) and with low coverage of spin-labeled ligands in the AuNP surface, as evident from the 3-line EPR spectra obtained.

The successful synthesis of large NPs with high coverage of spin labels made it possible to study their magnetic interactions.

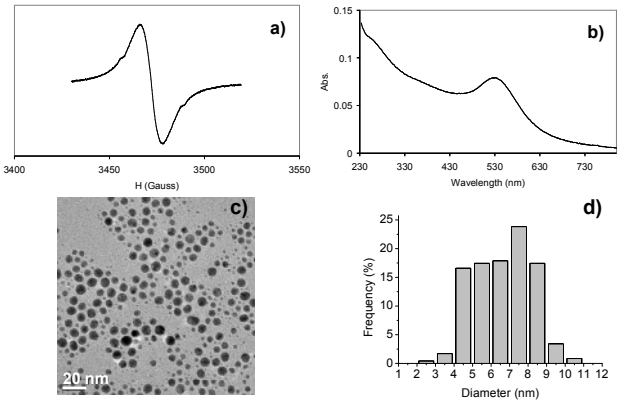

Figure 5. Characterization of nanoparticles 6. a) EPR spectrum in CH_2Cl_2 at room temperature, b) UV-Vis spectrum in CH_2Cl_2, c) TEM picture of AuNPs and d) core size distribution histograms of the nanoparticles.

The Thermogravimetric analyses (TGA) of NPs **3T**, **5T** and **6** showed that 27- 40 % of the total mass of nanoparticles is organic coating. From these data and TEM analysis we can estimate the number of radicals by nanoparticle and the packing density, which are too high according to the literature data reported (see the Supporting Information). However, these results support those obtained by EPR. The shape of the EPR spectra is very sensitive to the radical-radical interactions and these are directly related with the packing density. Therefore, a qualitative but unequivocally way to distinguish the packing density is to use the EPR spectroscopy,[26] a powerful tool to study spin labeled Au NPs.[44]

Magnetic properties of the high coverage gold nanoparticles. Gold nanoparticles 3T, 5T and 6 with high surface coverage of free radicals were studied in detail by EPR spectroscopy. These systems are characterised by a random distribution of labels between particles and on the particles and hence even for systems with high average coverage there are some isolated nitroxides. This could affect magnetic properties, as not all nitroxides interact with each other. However, the amount of these isolated nitroxides is very small and its contribution to the total spectra should be very small too, as we can see in the EPR shape of the spectra. A variable-temperature study was performed in the range 300 – 140 K, observing some broadening of the spectral line of all these materials with the decreased temperature. The EPR spectra for nanoparticles 6 at 300 and 140 K are shown in Figure 6b (see Figures S2 and S3 for similar spectra of nanoparticles 3T and 5T). At 140 K, an $|\Delta m_s| = 2$ transition was observed at half-field resulting from the dipolar interactions[45] (see Figure 6a). No $|\Delta m_s| = 3$ or other lower-field transitions could be observed. This is the first time that a forbidden transition was observed in the EPR spectra of spin-labeled nanoparticles. This forbidden transition gives direct evidence for

the presence of a high-spin state in these systems and therefore makes it possible to study the nature of the magnetic coupling between spins.

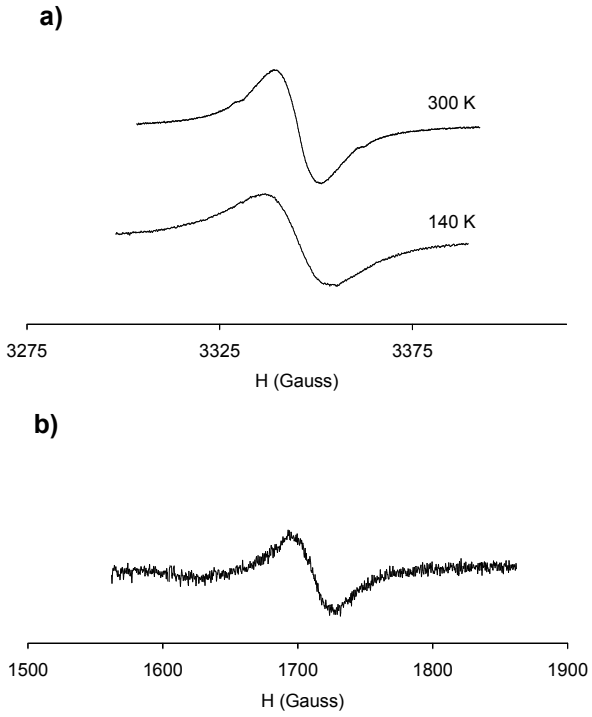

Figure 6. EPR spectra of nanoparticles 6 in dichloromethane. a) Spectra at 300 K and 140 K. b) $|\Delta m_s| = 2$ transition at half-field at 140 K.

Magnetic interactions in a paramagnetic compound are conventionally studied by SQUID magnetometry. Unfortunately, such studies require large amount of sample, particularly if the spin density is relatively low as in the case of organic radicals. However, we can make a semi-quantitative assessment of the magnetic interactions that take place in the nanoparticles by an EPR technique. The intensity of the forbidden EPR transition signal is proportional to the imaginary part of the magnetic susceptibility.[46] Therefore, the plot of I·T *vs.* T (where I is the spectrum intensity of the $|\Delta m_s| = 2$ transition) shows the same habit of the curve as in the usual

representation of $\chi \cdot T$ *vs.* T as measured by SQUID. According to the shape of the curve obtained, we can estimate the type of predominant magnetic interactions in the sample.

The intensity of the $|\Delta m_s| = 2$ transition signal (I) was measured in the 4-80 K temperature region. The corresponding I·T *vs.* T curve for nanoparticles 6 is shown in Figure 7. We can observe a decrease of the I·T value as the temperature decreases from 80 to 10 K. This behaviour is indicative of predominant antiferromagnetic interactions between the spin carriers. However, below 10 K, the trend changes abruptly, i.e. the I·T value increases with decreased temperature. This suggests that below this temperature, the interactions between the spin carriers could be predominantly ferromagnetic. The coexistence of dominant antiferromagnetic and weaker ferromagnetic interactions or *vice versa* has been observed in a few examples of purely organic radicals systems[47,48] or metal-organic radical-based systems[49,50] and in some inorganic compounds.[51-56]

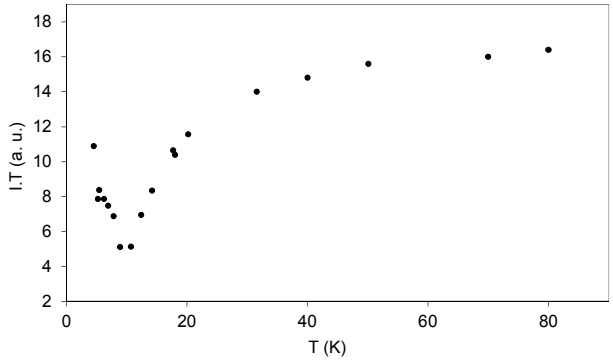

Figure 7. Dependence of the intensity of the half-field transition band $|\Delta m_s| = 2$ with temperature for nanoparticles 6.

Stability of the high-coverage spin-labelled gold nanoparticles. Gold nanoparticles 3T, 5T and 6 with high coverage of TEMPO-based radical ligands were reanalyzed by EPR and TEM after 1 year of storage at -18ºC under argon atmosphere. EPR spectroscopy showed that spin-

labeled ligands in all samples were quite stable because the spectral patterns were almost the same, always dominated by a broad line. Moreover, TEM microscopy did not show any change in the size core or distribution for all nanoparticles.

SUMMARY AND CONCLUSION

We have reported three different strategies for producing large Au nanoparticles with high coverage of a TEMPO-based ligand. Two methods followed a three-step procedure: preparation of gold nanoparticles, ligand-exchange reaction and a heat treatment in the solid state to enlarge the particles. A better protocol has been developed that makes it possible to obtain large nanoparticles with high spin label coverage in a single step and at room temperature, avoiding any heat treatment and with better results than in the three-step procedures. The nanoparticles thus prepared show an $|\Delta ms| = 2$ transition at half-field, which has never been observed in this kind of systems before and has allowed us to carry out an EPR study of the nature of the magnetic coupling between the spins. The study showed dominant antiferromagnetic interactions between radicals but at low temperatures a ferromagnetic contribution was observed.

AUTHOR INFORMATION

Corresponding Author

* Phone: 0034 935801853. Fax: 0034 935805729. E-mail: j.vidal@icmab.es

* Phone: 01904 322511. Fax: 01904 322516. E-mail: victor.chechik@york.ac.uk

Present Addresses

†*E. Badetti*. Università degli Studi di Padova, Dipartimento di Scienze Chimiche; Via Marzolo, 1, 35131; Padova, Italy.

Author Contributions

The manuscript was written through contributions of all authors. All authors have given approval to the final version of the manuscript.

ACKNOWLEDGMENT

This work was supported by the DGI grant CONSOLIDERC (CTQ2006-06333), CSIC-PIF RAPCAM (PIF-08-017-3), AGAUR (2009-SGR-00516) and DGI grant POMAs (CTQ2010-19501). CIBER-BBN is an initiative funded by the VI National R&D&i Plan 2008-2011, *Iniciativa Ingenio 2010, Consolider Program, CIBER Actions* and financed by the Instituto de Salud Carlos III with assistance from the *European Regional Development Fund*. We thank the UAB Microscopy service for their help in recording TEM images.

ASSOCIATED CONTENT

Supporting Information Available. Details of the nanoparticles synthesis, TEM, additional EPR data, EDX and TGA data. This information is available free of charge via the Internet at http://pubs.acs.org.

REFERENCES

(1) Suga, T.; Sugita, S.; Ohshiro, H.; Oyaizu, K.; Nishide, H. p- and n-Type Bipolar Redox-Active Radical Polymer: Toward Totally Organic Polymer-Based Rechargeable Devices with Variable Configuration. *Adv. Mater.* **2011**, *23*, 751–754.

(2) Barrales-Rienda, J. M.; Vidal-Gancedo, J. Thermodynamic Studies on poly N-(*n*-octadecyl)maleimide (PMI-18)/ Solvent Systems by Inverse Gas Chromatography with Capillary Columns. *Macromolecules* **1988**, *21*, 220–228.

(3) Bosman, A. W.; Janssen, R. A. J.; Meijer, E. W. Five Generations of Nitroxyl-Functionalized Dendrimers. *Macromolecules* **1997**, *30*, 3606–3611.
(4) Ottaviani, M. F.; Modelli, A.; Zeika, O.; Jockusch, S.; Moscatelli, A.; Turro, N. J. EPR Analysis and DFT Computations of a Series of Polynitroxides. *J. Phys. Chem. A* **2012**, *116*, 174–184.
(5) Badetti, E.; Lloveras, V.; Wurst, K.; Sebastián, R. M.; Caminade, A. M.; Majoral, J. P.; Veciana, J.; Vidal-Gancedo, J. Synthesis and Structural Characterization of a Dendrimer Model Compound Based on a Cyclotriphosphazene Core with TEMPO Radicals as Substituents. *Org. Lett.* **2013**, *15(14)*, 3490–3493.
(6) Templeton, A. C.; Hostetler, M. J.; Warmoth, E. K.; Chen, S.; Hartshorn, C. M.; Krishnamurthy, V. M.; Forbes, M. D. E.; Murray, R. W. Gateway Reactions to Diverse, Polyfunctional Monolayer-Protected Gold Clusters. *J. Am. Chem. Soc.* **1998**, *120*, 4845–4849.
(7) Ionita P., Caragheorgheopol A., Gilbert B.C., Chechik V. Dipole−Dipole Interactions in Spin-Labeled Au Nanoparticles as a Measure of Interspin Distances. *J. Phys. Chem. B* **2005**, *109(9)*, 3734–3742.
(8) Ionita, P.; Volkov, A.; Jeschke, G.; Chechik, V. Lateral Diffusion of Thiol Ligands on the Surface of Au Nanoparticles: An Electron Paramagnetic Resonance Study. *Anal. Chem.* **2008**, *80(1)*, 95–106.
(9) Zachary, M.; Chechik, V. Hopping of Thiolate Ligands between Au Nanoparticles Revealed by EPR Spectroscopy. *Angew. Chem. Int. Ed.* **2007**, *46(18)*, 3304–3307.
(10) Kaim, A.; Szydlowska, J.; Piotrowski, P.; Megiel, E. One-pot Synthesis of Gold Nanoparticles Densely Coated with Nitroxide Spins. *Polyhedron* **2012**, *46*, 119-123.
(11) Swiech, O.; Bilewicz, R.; Megiel, E. TEMPO Coated Au Nanoparticles: Synthesis and Tethering to Gold Surfaces. *RSC Adv.* **2013**, *3*, 5979–5986.
(12) Nagasaki, Y. Nitroxide Radicals and Nanoparticles: A Partnership for Nanomedicine Radical Delivery. *Therapeutic delivery* **2012**, *3(2)*, 1–15.
(13) Harada, G.; Sakurai, H.; Matsushita, M.; Izuoka, A.; Sugawara, T. Preparation and Characterization of Gold Nano-Particles Chemisorbed by π-Radical Thiols. *Chem. Lett.* **2002**, *31*, 1030–1031.
(14) Pasquato, L.; Pengo, P.; Scrimin, P. Functional Gold Nanoparticles for Recognition and Catalysis. *J. Mater. Chem.* **2004**, *14*, 3481–3487.
(15) Dreaden, E. C.; Alkilany, A. M.; Huang, X.; Murphy, C. J.; El-Sayed, M. A. The Golden Age: Gold Nanoparticles for Biomedicine. *Chem. Soc. Rev.* **2012**, *41*, 2740–2779.
(16) Boisselier, E.; Astruc, D. Gold Nanoparticles in Nanomedicine: Preparations, Imaging, Diagnostics, Therapies and Toxicity. *Chem. Soc. Rev.* **2009**, *38*, 1759–1782.
(17) Escosura-Muniz, A. De La; Sánchez-Espinel, C.; Díaz-Freitas, B.; González-Fernández, A.; Maltez-da Costa, M.; Merkozi, A. Rapid Identification and Quantification of Tumor Cells Using an Electrocatalytic Method Based on Gold Nanoparticles. *Anal. Chem.* **2009**, *81*, 10268–10274.
(18) Llevot, A.; Astruc, D. Applications of Vectorized Gold Nanoparticles to the Diagnosis and Therapy of Cancer. *Chem. Soc. Rev.* **2012**, *41*, 242–257.
(19) Huag, X.; Prashant, K. J.; El-Sayed, I. H.; El-Sayed, M. A. Gold Nanoparticles: Interesting Optical Properties and Recent Applications in Cancer Diagnostics and Therapy. *Nanomedicine* **2007**, *2*, 681–693.
(20) Caps, V. Les Nanoparticules d'Or en Catalyse d'Oxydation. *Actual. Chim.* **2010**, *337*, 18–22.

(21) Wang, X.; Ramstroem, O.; Yan, M. A. A Photochemically Initiated Chemistry for Coupling Underivatized Carbohydrates to Gold Nanoparticles. *J. Mater. Chem.* **2009**, *19*, 8944–8949.
(22) Sugawara, T.; Matsushit, M. M. Spintronics in Organic π-Electronic Systems. *J. Mater. Chem.* **2009**, *19*, 1738–1753.
(23) Brust, M.; Walter, M.; Bethell, D.; Schiffrin, D. J.; Whyman, R. Synthesis of Thiol-derivatised Gold Nanoparticles in a Two-phase Liquid-Liquid System. *J. Chem. Soc., Chem. Commun.* **1994**, 801–802.
(24) Daniel, M. C.; Astruc, D. Gold Nanoparticles: Assembly, Supramolecular Chemistry, Quantum-Size-Related Properties, and Applications toward Biology, Catalysis, and Nanotechnology. *Chem. Rev.* **2004**, *104*, 293–346.
(25) Ionita, P.; Caragheorgheopol, A.; Gilbert, B. C.; Chechik, V. EPR Study of a Place-Exchange Reaction on Au Nanoparticles: Two Branches of a Disulfide Molecule Do Not Adsorb Adjacent to Each Other. *J. Am. Chem. Soc.* **2002**, *124*, 9048–9049.
(26) Chechik, V.; Wellsted, H. J.; Korte, A.; Gilbert, B. C.; Caldararu, H.; Ionita, P.; Caragheorgheopol, A. Spin-Labelled Au Nanoparticles. *Faraday Discuss.* **2004**, *125*, 279–291.
(27) Wellsted, H.; Sitsen, E.; Caragheorgheopol, A.; Chechik, V. Polydisperse Composition of Mixed Monolayer-Protected, Spin-Labeled Au Nanoparticles. *Anal. Chem.* **2004**, *76*, 2010–2016.
(28) Shon, Y. S.; Mazzitelli, C.; Murray, R. W. Unsymmetrical Disulfides and Thiol Mixtures Produce Different Mixed Monolayer-Protected Gold Clusters. *Langmuir* **2001**, *17*, 7735–7741.
(29) Zheng N.; Fan J.; Stucky G. D. One-Step One-Phase Synthesis of Monodisperse Noble-Metallic Nanoparticles and Their Colloidal Crystals. *J. Am. Chem. Soc.* **2006**, *128,* 6550–6551.
(30) Stoeva S. I.; Zaikovski V.; Prasad B. L. V.; Stoimenov P. K.; Sorensen C. M.; Klabunde K. J. Reversible Transformations of Gold Nanoparticle Morphology. *Langmuir* **2005**, *21*, 10280–10283.
(31) Barnard A. S.; Lin X. M.; Curtiss L. A. Equilibrium Morphology of Face-Centered Cubic Gold Nanoparticles >3 nm and the Shape Changes Induced by Temperature. *J. Phys. Chem. B* **2005**, *109*, 24465–24472.
(32) Yong K. T.; Sahoo Y.; Choudhury K. R.; Swihart M. T.; Minter J. R.; Prasad P. N. Control of the Morphology and Size of PbS Nanowires Using Gold Nanoparticles. *Chem. Mater.* **2006**, *18*, 5965–5972.
(33) Rodríguez-Fernández J.; Pérez-Juste J.; García de Abajo F. J.; Liz-Marzan L. M. Seeded Growth of Submicron Au Colloids with Quadrupole Plasmon Resonance Modes. *Langmuir* **2006**, *22*, 7007–7010.
(34) Park, J.; Lee, E.; Hwang, N. M.; Kang, M.; Kim, S. C.; Hwang, Y.; Park, J. G.; Noh, H. J.; Kim, J. Y.; Park, J. H.; et al. One-Nanometer-Scale Size-Controlled Synthesis of Monodisperse Magnetic Iron Oxide Nanoparticles. *Angew. Chem. Int. Ed.* **2005**, *44*, 2872–2877.
(35) Yang, Y.; Wang, W.; Jinru, L. Precise Size Control of Hydrophobic Gold Nanoparticles using Cooperative Effect of Refluxing Ripening and Seeding Growth. *Nanotechnology* **2008**, *19*, 175603–175613.
(36) Link, S.; El-Sayed, M. A. Size and Temperature Dependence of the Plasmon Absorption of Colloidal Gold Nanoparticles. *J. Phys. Chem. B* **1999**, *103*, 4212–4217.
(37) Álvarez, M. M.; Khoury, J. T.; Schaaff, T. G.; Shafigullin, M. N.; Vezmar, I.; Whetten, R. L. Optical Absorption Spectra of Nanocrystal Gold Molecules. *J. Phys. Chem. B* **1997**, *101*, 3706–3712.

(38) Hostetler, M. J.; Wingate, J. E.; Zhong, C. J.; Harris, J. E.; Vachet, R. W.; Clark, M. R.; Londono, J. D.; Green, S. J.; Stokes, J. J.; Wignall, G. D.; et al. Alkanethiolate Gold Cluster Molecules with Core Diameters from 1.5 to 5.2 nm: Core and Monolayer Properties as a Function of Core Size. *Langmuir* **1998**, *14*, 17–30.
(39) Tranishi T.; Hasegawa S.; Shimizu T.; Miyake M. Heat-Induced Size Evolution of Gold Nanoparticles in the Solid State. *Adv. Mater.* **2001**, *13*, 1699–1701.
(40) Fink, J.; Kiely, C.J.; Bethell, D.; Schiffrin D. J. Self-Organization of Nanosized Gold Particles. *Chem. Mater.* **1998**, *10*, 922–926.
(41) Weare, W. W.; Reed, S. M.; Warner, M. G.; Hutchison, J. E. Improved Synthesis of Small ($d_{CORE} \approx 1.5$ nm) Phosphine-Stabilized Gold Nanoparticles. *J. Am. Chem. Soc.* **2000**, *122*, 12890–12891.
(42) Link, S.; El-Sayed, M. A. Shape and Size Dependence of Radiative, Non-Radiative and Photothermal Properties of Gold Nanocrystals. *Int. Rev. Phys. Chem.* **2000**, *19 (3)*, 409–453.
(43) Alger, R. S. *Electron Paramagnetic Resonance: Techniques and Applications*; Interscience Publishers: New York, 1968.
(44) Lucarini, M; Pasquato, L. ESR Spectroscopy as a Tool to Investigate the Properties of Self-Assembled Monolayers Protecting Gold Nanoparticles. *Nanoscale* **2010**, *2*, 668-676.
(45) Eaton, S. S.; More, K. M.; Savant, B. M.; Eaton, G. R. Use of the ESR Half-Field Transition to Determine the Interspin Distance and the Orientation of the Interspin Vector in Systems with Two Unpaired Electrons. *J. Am. Chem. Soc.* **1983**, *105*, 6560–6567.
(46) Wertz, J. E.; Bolton, J. R. *Electron Spin Resonance*. Chapman: New York, 1972.
(47) Sutter, J. P.; Lang, A.; Kahn, O.; Paulsen, C.; Ouahab, L.; Pei, Y. Ferromagnetic Interactions, and Metamagnetic Behaviour of 4,5-dimethyl- 1,2,4-triazole-nitronyl-nitroxide. *J. Magn. Magn. Mater.* **1997**, *171*, 147–152.
(48) Kasumov, V. T.; Uçar, I.; Bulut, A.; Yerli, Y. Synthesis, Crystal Structure and Intermolecular Magnetic Interactions of a New N-TEMPO-3,5-di-tert-butylsalicylaldimine Radical. *Solid State Sci.* **2011**, *13*, 1852–1857.
(49) Maspoch, D.; Domingo, N.; Ruiz-Molina, D.; Wurst, K.; Hernández, J. M.; Vaughan, G.; Rovira, C.; Lloret, F.; Tejada, J.; Veciana, J. Coexistence of Ferro- and Antiferromagnetic Interactions in a Metal–Organic Radical-Based (6,3)-Helical Network with Large Channels. *Chem. Commun.* **2005**, 5035–5037.
(50) Roques, N.; Maspoch, D.; Luis, F.; Camón, A.; Wurst, K.; Datcu, A.; Rovira, C.; Ruiz-Molina, D.; Veciana, J. A Hexacarboxylic Open-Shell Building Block: Synthesis, Structure and Magnetism of a Three-Dimensional Metal–Radical Framework. *J. Mater. Chem.* **2008**, *18*, 98–108.
(51) Clemente-Juan, J. M.; Coronado, E.; Forment-Aliaga, A.; Galán-Mascarós, J. R.; Giménez-Saiz, C.; Gómez-García, C. J. A New Heptanuclear Cobalt(II) Cluster Encapsulated in a Novel Heteropolyoxometalate Topology: Synthesis, Structure, and Magnetic Properties of $[Co_7(H_2O)_2(OH)_2P_2W_{25}O_{94}]^{16-}$. *Inorg. Chem.* **2004**, *43*, 2689–2694.
(52) de Pedro, I.; Rojo, J. M.; Lezama, L.; Rojo, T. Spectroscopic and Magnetic Properties of $Co_{1.7}Mn_{0.3}(OH)PO_4$. *Z. Anorg. Allg. Chem.* **2007**, *633*, 1847–1852.
(53) Bazán, B.; Mesa, J. L.; Peña, A.; Legarra, E.; Pizarro, J. L.; Arriortua, M. I.; Rojo, T. Structural Characterization, Thermal, Spectroscopic and Magnetic Studies of the $(C_3H_{12}N_2)_{0.75}[Mn_{1.50}{}^{II}Fe_{1.50}{}^{III}(AsO_4)F_6]$ and $(C_3H_{12}N_2)_{0.75}[Co_{1.50}{}^{II}Fe_{1.50}{}^{III}(AsO_4)F_6]$ compounds. *Mater. Res. Bull.* **2008**, *43*, 1307–1320.

(54) Yang, F.; Li, B.; Xu, W.; Li, G.; Zhou, Q.; Hua, J.; Shi, Z.; Feng, S. Two Metal–Organic Frameworks Constructed from One-Dimensional Cobalt(II) Ferrimagnetic Chains with Alternating Antiferromagnetic/Ferromagnetic and AF/AF/FM Interaction: Synthesis, Structures, and Magnetic Properties. *Inorg. Chem.* **2012**, *51*, 6813–6820.
(55) Zhanga, L.; Gaoa, W.; Wua, Q.; Sua, Q.; Zhanga, J.; Mua, Y. Synthesis and Characterization of Chiral Trinuclear Cobalt and Nickel Complexes Supported by Binaphthol-Derived bis(salicylaldimine) Ligands. *J. Coord. Chem.* **2013**, *66*, 3182–3192.
(56) Zhao, J.; Li, D. S.; Wu, Y. P.; Yang, J. J.; Dong, W. W.; Zou, K. A Rare Pentanuclear CuII-Based Coordination Framework Exhibiting Coexistence of Antiferromagnetic and Ferromagnetic Couplings. *Inorg. Chem. Commun.* **2013**, *35*, 61–64.

TOC